Glacial climate instability controlled by atmospheric CO_2

Xu Zhang[1,2]*, Gregor Knorr[1,3], Gerrit Lohmann[1,4], Stephen Barker[3]

[1]Alfred Wegener Institute Helmholtz Centre for Polar and Marine Research,
Bussestr. 24, D-27570, Germany

[2]Laboratory for Marine Geology, National Laboratory for Marine Science and Technology,
Qingdao, 266001, China

[3]School of Earth and Ocean Sciences, Cardiff University, Cardiff, UK

[4]University of Bremen, Bremen, Germany

*Correspondence to: Xu Zhang (xu.zhang@awi.de)

Glacial climate is marked by abrupt, millennial scale climate changes, known as Dansgaard-Oeschger (DO) cycles. The most pronounced stadial coolings are known as Heinrich events and are associated with massive iceberg discharges to the North Atlantic. These events have been linked to variations in the strength of the Atlantic meridional overturning circulation (AMOC). However, the factors that lead to abrupt transitions between strong and weak circulation regimes remain unclear. Here we show that, in a fully coupled atmosphere-ocean model, gradual changes in atmospheric CO_2 concentrations can trigger abrupt climate changes associated with a regime of AMOC bi-stability under intermediate glacial conditions. We find that CO_2 changes alter the transport of atmospheric moisture across Central America, which modulates the freshwater budget of the North Atlantic and the stability of deep-water formation. In our simulations, a CO_2 change of about 15 ppmv is sufficient to cause transitions between a weak stadial and a strong interstadial circulation mode. This value is comparable to the CO_2 change seen during Heinrich-DO cycles. Because changes in the AMOC are thought to alter atmospheric CO_2 concentrations, we infer that CO_2 may serve as a negative feedback to transitions between strong and weak circulation modes.

Abrupt climate changes associated with DO events as recorded in Greenland ice cores are characterized by rapid warming from stadial to interstadial conditions. This is followed by a phase of gradual cooling before an abrupt return to cold stadial conditions[1,2]. A common explanation for these transitions involves changes in the AMOC[3], perhaps controlled by freshwater perturbation[(e.g. 4,5)] and/or Northern Hemisphere ice sheet changes[(e.g. 6–8)]. To reproduce the abrupt transitions into and out of cold conditions across the North Atlantic (i.e. AMOC weak or "off" mode[3]), a common trigger mechanism is related to the timing of North Atlantic freshwater perturbations[9,10] that is mainly motivated by unequivocal ice-rafting events during Heinrich Stadials (HS)[11]. However, recent studies suggest that the Heinrich ice-surging

events are in fact triggered by sea subsurface warming associated with an AMOC slow-down[12,13]. Furthermore, the duration of ice-rafting events does not systematically coincide with the beginning and end of the pronounced cold conditions during HS[14,15]. This evidence thus challenges the current understanding of glacial AMOC stability[5,8], suggesting the existence of additional control factors that should be invoked to explain abrupt millennial scale variability in climate records. In contrast to the North, the rapid climate transitions are characterized by inter-hemispheric anti-phased variability with more gradual changes in southern high-latitudes[16] due to the thermal bipolar seesaw effect[17]. This Antarctic-style climate variability[16], represents a pervasive signal on a global scale and shares a close correspondence with changes in atmospheric CO_2[18,19]. In addition, numerous paleoclimate records clearly show that D-O activity is most pronounced when both global ice volume and atmospheric CO_2 levels are intermediate between glacial and interglacial extremes[1,2,6,20,21]. Taken together this evidence has led to suggestions that gradual changes in background climate, associated with variations in atmospheric CO_2, have the potential to explain the occurrence of abrupt climate shifts during ice ages[18,19,22,23].

Gradual CO_2 changes as a forcing factor

With aid of the comprehensive coupled climate model COSMOS[8,9] we explore the governing mechanism of AMOC stability associated with atmospheric CO_2 changes. Two experiments were conducted with gradual changes in atmospheric CO_2 under intermediate (CO2_Hys) and maximum (LGM_0.15_CO2) ice volumes (Table S1). In experiment CO2_Hys, atmospheric CO_2 concentration was linearly changed between 185 and 239 ppm at a rate of 0.02 ppm/year to mimic millennial-scale CO_2 variations during glacials[24]. This forcing is sufficiently weak as to simulate a quasi-equilibrium response of the climate system to changing CO_2. The prescribed (intermediate) ice volume is equivalent to a sea level of ~42 m below present-day conditions[8]

(Table S1), equivalent to an early stage of the last glacial cycle[25]. Other boundary conditions were kept constant at Last Glacial Maximum (LGM) conditions[9] (Methods).

In experiment LGM_0.15_CO2, an equilibrated weak AMOC mode forced by persistent freshwater flux (0.15 Sv, Sv=10^6 m^3/s) under LGM conditions[9] (Table S1) serves as the initial state (Fig. S1). The freshwater perturbation can be considered to represent North Atlantic (NA) meltwater input associated with surface mass balance of the surrounding ice sheets and/or freshwater injection associated with ice-surging events during Heinrich Stadials. The atmospheric CO_2 concentration varies gradually between 185ppm and 245ppm at a rate of 0.05 ppm/year, representative of observed rate of CO_2 changes during the last deglaciation[26]. This setup provides a surrogate for Heinrich stadial-interstadial transitions during glacial periods (especially during the last deglaciation) to test the robustness of the simulated changes in experiment CO2_Hys. As shown later, in both experiments the AMOC shares similar characteristics in response to the CO_2 changes (Fig. 1).

AMOC response to gradual CO_2 changes

The simulated glacial ocean circulation (prior to transient forcing) is characterized by a weak AMOC mode with cold stadial conditions in the north (Fig. 1a-c). In response to a linear increase in CO_2 concentration, surface air temperature (SAT) over the northern high latitudes experiences abrupt warming, along with a rapid AMOC reorganization from a weak stadial to a strong inter-stadial mode (interval A-B in Fig. 1a, and S2a). The opposite occurs in the scenario with decreasing atmospheric CO_2 (interval C-D in Fig. 1a, and S2a). The simulated magnitude of abrupt Greenland warming/cooling is much smaller than the observed, probably due to the underestimated sea ice retreat in the Nordic Seas[27] in the strong AMOC mode of experiment CO2_Hys (Fig. S3). Nevertheless, changes in sea surface temperature in the North Atlantic are well captured between the two contrasting climate states (Figs. S4-5). In contrast to the abrupt climate shifts in the north, the simulated Antarctic and global SATs vary more

gradually, in line with the CO_2 forcing (Figs. 1a-d and S2a, g). This gradual signature is also reflected in the SAT trend of the northern high latitudes prior to the abrupt transitions (i.e. the period A-B and C-D in Fig. 1a and S2a). The AMOC itself does not show this gradual trend and instead maintains a relatively constant strength before experiencing an abrupt shift (Fig. 1a-c). In addition, it is worthy to note that changes in CO_2 concentration (~15 ppm) that account for the co-existence of two distinct glacial ocean states (Fig. 2a) are of comparable magnitude as real millennial-scale CO_2 variations recorded during glacial cycles[20,24] (Fig. 1a, b). Overall, the simulated changes (Figs. 1a-e and S2-5) share many characteristics with empirical evidence of millennial-scale Heinrich-DO variability[16,20,24,28,29].

We now focus on the first 2000 model years of experiment CO2_Hys while AMOC is in its weak mode to illustrate the underlying dynamics of the abrupt AMOC amplification at the end of interval A-B in Fig. 1a. It is known that the sinking branch of the AMOC closely relates to the vertical stratification (i.e. vertical density gradient) that is mainly controlled by ocean temperature and salinity in the main convection sites of the North Atlantic. At the sea surface, the background warming (~0.25 °C/ka), which is linked to the CO_2 increase, decreases the surface water density in the northeastern North Atlantic (NENA, the main convection sites, 50–65°N, 10–30°W). This strengthens the vertical stratification and thermally stabilizes the weak mode of AMOC (Fig. 2c). Nevertheless, the thermal impact on surface density is overcome by a synchronous haline effect (i.e. the surface water salinity increase at a rate of ~0.07 psu/ka, see below). This offsets the warming effect and causes a net increase in the surface water density at a rate of ~0.04 kg/m^3/ka (Fig. 2b, d). This relationship is also detected at the subsurface in the NENA, leading to water density increase at a slower rate (i.e. ~0.01 kg/m^3/ka) than the surface density increase (Fig. 2b, d). This vertical contrast in rates of water density change highlights the importance of a top-down de-stratification via surface salinization, eventually leading to an abrupt AMOC recovery.

Of particular importance to explain the surface salinity increase in the NENA are changes in meridional freshwater transport (MFT) in the North Atlantic[30]. We find that an increase in the northward salinity transport (negative MFT in Fig. 1g) dominates over local surface freshening (~0.0011 Sv/ka) associated with increased net precipitation in the NENA (Fig. 2e). Along with the CO_2 increase, the MFT during the weak AMOC phase gradually decreases by ~0.2 Sv across the boundary between the subtropical and subpolar gyre in the North Atlantic (~43°N) prior to the rapid AMOC recovery (Fig. 1g). Since the strength of the AMOC during this interval is relatively stable (Fig. 1b), the weakened MFT can be mainly attributed to an increase in the subtropical sea surface salinity in the North Atlantic (see below). This causes a saltier northward AMOC branch that feeds into the NENA via the North Atlantic subtropical gyre. Changes in the freshwater import across the southern boundary of the Atlantic catchment area at ~29°S[31,32] and the equatorial Atlantic Ocean are determined to be of minor importance (Fig. S2j, k).

A key mechanism responsible for changes in the subtropical sea surface salinity is the zonal atmospheric moisture transport across Central America. Previous data and model studies suggest that a southward shift of the Intertropical Convergence Zone (ITCZ) is responsible for the salinity increase in the western subtropical North Atlantic (WSNA, 60-90°W, 10°N-30°N) during cold stadial periods[28,30,33–35]. This is presumed to be a precondition for NADW formation to abruptly return to warm interstadial conditions with a strong AMOC mode[28,34]. In our model, the southward-displaced ITCZ (Fig. S4b) and salinity increase in the WSNA (Fig. S5a) are well captured in the simulated strong-to-weak AMOC transition. However, the salinity increase stops after the transition is complete (Fig. S6). As a consequence, the stationary salinity anomaly is not sufficient to enable an abrupt resumption of the AMOC (Fig. 3a), as shown in simulations LIS_0.2 and LGM_0.15 (Fig. S1 and Table S1) that are, respectively, equivalent to experiments CO2_Hys and LGM_0.15_CO2 but without CO_2 changes.

However, once a CO_2 increase is additionally imposed to the cold stadial conditions (e.g. interval A-B in CO2_Hys), trade winds over the Central America are further enhanced by the strengthened sea-level pressure gradient between the eastern Equatorial Pacific (EEP, 90-120°W, 5-15°N) and the WSNA (Figs. 2e and 3b). This is a consequence of the associated El Nino-like warming pattern in the Pacific and Atlantic with a relatively stronger warming in the EEP than the WSNA (Fig. S7). These warming characteristics are consistent with sea surface temperature responses in global warming scenarios as simulated in climate projections using CMIP5 models[36]. In addition to increased evaporation over the WSNA due to the Clausius-Clapeyron relation, the enhanced trade winds boost the atmospheric moisture transport, reducing (increasing) the surface water salinity in the EEP (WSNA) (Figs. 1f and S2h, i).

To further test this, we analyse the observed CO_2-$Salinity_{EEP}$ relationship during HS intervals that are accompanied with CO_2 increases in the last 90 thousand years[20,37,38] (Figs. S8-9). As shown in Fig. S10, rising CO_2 did appear to coincide with declining salinity in the EEP[38] (Fig. S9). These findings thus suggest that changes in the atmospheric moisture transport across Central America, driven by a gradual CO_2 increase, can stimulate an AMOC recovery from cold HS conditions by increasing salinity in the subtropical North Atlantic (Fig. 3b-c). This also reconciles previous controversies regarding the roles played by the southward-shifted ITCZ during cold Heinrich stadials on the subsequent abrupt transitions to warm interstadials[28,34,38].

In addition to the haline impact, decline in sea ice concentration (SIC) in the North Atlantic, as a positive feedback to AMOC recovery[8], helps to reinforce abrupt AMOC changes. In CO2_Hys the reduction in the SIC (Fig. 1d) increases the ocean surface area that is exposed to the cold atmosphere. This 'area' effect overcompensates for the reduced heat loss due to a weakened air-sea surface temperature contrast and promotes an enhanced net heat loss to the atmosphere over the NENA (Fig. S2b, c). As a consequence, the warmer SAT enhances the local cyclonic wind stress that strengthens the North Atlantic Subpolar Gyre (Figs. 2e and S2a,

e). This in turn strengthens the local sea ice variability, shifting its probability distribution from single peak to double peak distribution prior to the AMOC resumption (Fig. S10). It is important to note that a sea-ice free mode already exists in the key convection sites of the North Atlantic as the AMOC is still in its weak mode. Therefore, we infer that changes in SIC alone are not the final trigger for the AMOC recovery. Once the AMOC recovery is triggered by changes in large-scale salinity advection, the atmospheric responses associated with the sea-ice reduction will boost a northward transport of surface water with a relatively high salinity from the south-eastern subpolar regions to the convection sites (Figs. 2b and S2d, S11). This deepens vertical mixing with underlying warmer water masses in the NENA, leading to an additional reduction in the SIC (Figs. 1e and S2a, f). The positive local atmosphere-ocean-sea ice feedback mechanisms superposed on the larger-scale salinity advection feedback operate to abruptly return NADW formation to a vigorous interstadial mode from cold stadial conditions as atmospheric CO_2 increases.

AMOC response to CO_2 change in the presence of NA hosing

The characteristic mechanisms and feedbacks that occur in response to CO_2 changes, leading to shifts in the mode of AMOC, also operate in the presence of positive freshwater perturbations to the North Atlantic (experiment LGM_0.15_CO2) (Figs. 1h-n, and S12-13). This indicates that the proposed mechanism can overcome the negative effect of persistent NA freshwater input on AMOC strength after a CO_2 increase of ~40ppm from the peak glacial level (185ppm), ultimately triggering an abrupt warming in the North (perhaps analogous to the sequence of events leading to the Bølling-Allerød (BA) and earlier HS-interstadial transitions). This further adds credence to the robustness of our results that are derived from the model without ice sheet dynamics, since diagnosed meltwater fluxes associated with changes in surface mass balance of the ice sheet are around 0.06 Sv during the interval A-B of experiment CO2_Hys. In addition, AMOC variability is characterized by increasing variance and autocorrelation in experiment

LGM_0.15_CO2 as the threshold is approached during the transition from a strong to a weak AMOC mode (Fig. 1 h-n). This feature, although shorter than non-Heinrich-DO events during the Marine Isotope Stage (MIS) 3 (e.g. DO events 5-7)[1], provides a potential approach to explain their occurrence[39] , but requires further investigation in the future.

AMOC stability and glacial climate

In contrast to previous studies[22,23], the model used in this study, with more advanced climate physics, enables us to elaborate on the comprehensive dynamics of mechanisms associated with changes in atmospheric CO_2 to explain millennial-scale variability and abrupt climate transitions during glacial periods. As a consequence of CO_2 changes, variations in the freshwater budget of the North Atlantic associated with the interoceanic atmospheric moisture transport across Central America represent a crucial control for the stability of glacial climate by providing a natural source of "freshwater perturbation" to the North Atlantic, thereby complementing previous concepts[5].

In combination with previous knowledge of the stability of glacial climate[5,8], we synthesize a concept to account for a broader spectrum of abrupt climate changes as documented in global climate archives (Fig. 4). As shown in the conceptual AMOC stability diagrams, both LGM ice volume and interglacial atmospheric CO_2 concentrations are accompanied by a strong mono-stable AMOC, reflecting the dominant role of ice volume under peak glacial conditions and atmospheric CO_2 during interglacial periods (Fig. 4). The interplay between changes in ice volume and atmospheric CO_2 therefore determines that windows of AMOC bi-stability will exist during intermediate conditions between peak glacial and interglacial states. For example, MIS 3 was characterized by pronounced millennial scale climate activity while the LGM and Holocene interglacial were not. Only within a window of bi-stability can temporary perturbations (e.g. CO_2, freshwater, solar irradiance, etc.) have a longer-term persistent effect on climate beyond the duration of the perturbation itself. Importantly, our analysis also shows

that gradual changes in atmospheric CO_2 can act as a trigger of abrupt climate changes. Moreover because millennial-scale changes in CO_2 are themselves thought to be driven in part by changes in the AMOC (with a weakened AMOC giving rise to a gradual rise in CO_2 and vice versa)[40], our results suggest that CO_2 might represent an internal feedback agent to AMOC changes[19] by promoting spontaneous transitions between contrasting climate states without the need for processes like ice rafting events across the North Atlantic[15,18]. More specifically, such an internal link can be characterized by rising CO_2 during Heinrich Stadial cold events triggering abrupt transitions to warm conditions and decreasing CO_2 during warm events, leading to abrupt cooling transitions. Therefore, CO_2 might provide a negative feedback on AMOC-induced climate shifts. We note that this mechanism may not account for non-H-DO variability although feasibly an analogous process may be at work for these 'smaller' events[18,19].

Our framework also indicates that during deglaciation the bi-stable window would be established only after ice volume has started to decrease but before peak interglacial CO_2 levels are achieved. For example, recovery of the AMOC during the BA warming occurred relatively early within Termination 1 (T1), before atmospheric CO_2 had attained its interglacial level and while the system was within its window of bi- stability, thus enabling a return to a weak mode of AMOC during the Younger Dryas (YD). By analogy during glacial inception a bi-stable AMOC regime only occurs after atmospheric CO_2 has declined from peak interglacial CO_2 levels and before ice volume has reached full glacial values.

Although the exact position of the simulated bi-stable AMOC windows with respect to ice volume[8] and atmospheric CO_2 might be different among climate models, the combined framework that is derived from our model can provide a systemic understanding of their relative roles within glacial-interglacial cycles (Fig. 4). In future studies of glacial-interglacial and millennial scale climate variability, the processes and feedbacks invoked here might serve as a basis to identify principal triggering mechanisms and forcing agents in both high-resolution

climate records and coupled climate model simulations that include carbon cycle dynamics and interactive ice sheet components.

References:

1. Dansgaard, W. *et al.* Evidence for general instability of past climate from a 250-kyr ice-core record. *Nature* **364,** 218–220 (1993).
2. Barker, S. *et al.* 800,000 Years of Abrupt Climate Variability. *Science* **334,** 347–351 (2011).
3. Rahmstorf, S. Ocean circulation and climate during the past 120,000 years. *Nature* **419,** 207–214 (2002).
4. Stommel, H. Thermohaline convection with two stable regimes of flow. *Tellus* **13,** 224–230 (1961).
5. Ganopolski, A. & Rahmstorf, S. Rapid changes of glacial climate simulated in a coupled climate model. *Nature* **409,** 153–158 (2001).
6. McManus, J. F., Oppo, D. W. & Cullen, J. L. A 0.5-Million-Year Record of Millennial-Scale Climate Variability in the North Atlantic. *Science* **283,** 971–975 (1999).
7. Wunsch, C. Abrupt climate change: an alternative view. *Q. Res.* **65,** 191 (2006).
8. Zhang, X., Lohmann, G., Knorr, G. & Purcell, C. Abrupt glacial climate shifts controlled by ice sheet changes. *Nature* **512,** 290–294 (2014).
9. Zhang, X., Lohmann, G., Knorr, G. & Xu, X. Different ocean states and transient characteristics in Last Glacial Maximum simulations and implications for deglaciation. *Clim. Past* **9,** 2319–2333 (2013).
10. Menviel, L., Timmermann, A., Friedrich, T. & England, M. H. Hindcasting the continuum of Dansgaard-Oeschger variability: Mechanisms, patterns and timing. *Clim. Past* **10,** 63–77 (2014).
11. Hemming, S. Heinrich Events: Massive Late Pleistocene Detritus Layers of the North

Atlantic and their global Climate Imprint. *Rev. Geophys.* **42,** RG1005 (2004).

12. Marcott, S. A. *et al.* Ice-shelf collapse from subsurface warming as a trigger for Heinrich events. *Proc. Natl. Acad. Sci.* **108,** 13415–9 (2011).

13. Bassis, J. N., Petersen, S. V. & Mac Cathles, L. Heinrich events triggered by ocean forcing and modulated by isostatic adjustment. *Nature* **542,** 332–334 (2017).

14. Bond, G. *et al.* A Pervasive Millennial-Scale Cycle in North Atlantic Holocene and Glacial Climates. *Science* **278,** 1257–1266 (1997).

15. Barker, S. *et al.* Icebergs not the trigger for North Atlantic cold events. *Nature* **520,** 333–336 (2015).

16. Jouzel, J. *et al.* Orbital and millennial Antarctic climate variability over the past 800,000 years. *Science* **317,** 793–796 (2007).

17. Stocker, T. F. & Johnsen, S. J. A minimum thermodynamic model for the bipolar seesaw. *Paleoceanography* **18,** 1–9 (2003).

18. Barker, S. & Knorr, G. A paleo-perspective on the AMOC as a tipping element. *PAGES News* **24,** 14–15 (2016).

19. Barker, S. & Knorr, G. Antarctic climate signature in the Greenland ice core record. *Proc. Natl. Acad. Sci.* **104,** 17278–17282 (2007).

20. Bereiter, B. *et al.* Revision of the EPICA Dome C CO2 record from 800 to 600 kyr before present. *Geophys. Res. Lett.* **42,** 1–8 (2015).

21. Kawamura, K. *et al.* State dependence of climatic instability over the past 720,000 years from Antarctic ice cores and climate modeling. *Sci. Adv.* **3,** 1–14 (2017).

22. Knorr, G. & Lohmann, G. Rapid transitions in the Atlantic thermohaline circulation triggered by global warming and meltwater during the last deglaciation. *Geochemistry Geophys. Geosystems* **8,** Q12006 (2007).

23. Banderas, R., Alvarez-Solas, J., Robinson, A. & Montoya, M. An interhemispheric mechanism for glacial abrupt climate change. *Clim. Dyn.* **44,** 2897–2908 (2014).

24. Ahn, J. & Brook, E. J. Siple Dome ice reveals two modes of millennial CO2 change during the last ice age. *Nat. Commun.* **5,** 3723 (2014).

25. Grant, K. M. *et al.* Rapid coupling between ice volume and polar temperature over the past 150,000 years. *Nature* **491,** 744–747 (2012).

26. Marcott, S. A. *et al.* Centennial-scale changes in the global carbon cycle during the last deglaciation. *Nature* **514,** 616–619 (2014).

27. Li, C., Battisti, D. S. & Bitz, C. M. Can North Atlantic Sea Ice Anomalies Account for Dansgaard–Oeschger Climate Signals?. *J. Clim.* **23,** 5457–5475 (2010).

28. Peterson, L. C., Haug, G. H., Hughen, K. A. & Roehl, U. Rapid Changes in the Hydrologic Cycle of the Tropical Atlantic During the Last Glacial. *Science* **290,** 1947–1951 (2000).

29. Voelker, A. H. L. Global distribution of centennial-scale records for Marine Isotope Stage (MIS) 3: a database. *Quat. Sci. Rev.* **21,** 1185–1212 (2002).

30. Lohmann, G. Atmospheric and oceanic freshwater transport during weak Atlantic overturning circulation. *Tellus* **5,** 438–449 (2003).

31. Rahmstorf, S. On the freshwater forcing and transport of the Atlantic thermohaline circulation. *Clim. Dyn.* 799–811 (1996).

32. Knorr, G. & Lohmann, G. Southern Ocean origin for the resumption of Atlantic thermohaline circulation during deglaciation. *Nature* **424,** 532–536 (2003).

33. Broecker, W. S., Bond, G., Klas, M., Bonani, G. & Wolfli, W. A Salt Oscillator in the Glacial Atlantic? 1. The Concept. *Paleoceanography* **5,** 469–477 (1990).

34. Schmidt, M. W., Vautravers, M. J. & Spero, H. J. Rapid subtropical North Atlantic salinity oscillations across Dansgaard-Oeschger cycles. *Nature* **443,** 561–564 (2006).

35. Zaucker, F. & Broecker, W. S. The influence of atmospheric moisture transport on the fresh water balance of the Atlantic drainage basin: General circulation model simulations and observations. *J. Geophys. Res.* **97,** 2765 (1992).

312 36. Collins, M. *et al.* Long-term Climate Change: Projections, Commitments and
313 Irreversibility. *Clim. Chang. 2013 Phys. Sci. Basis. Contrib. Work. Gr. I to Fifth Assess.*
314 *Rep. Intergov. Panel Clim. Chang.* 1029–1136 (2013).
315 doi:10.1017/CBO9781107415324.024
316 37. Ahn, J. & Brook, E. J. Atmospheric CO_2 and climate on millennial time scales during
317 the last glacial period. *Science* **83,** 83–85 (2008).
318 38. Leduc, G. *et al.* Moisture transport across Central America as a positive feedback on
319 abrupt climatic changes. *Nature* **445,** 908–911 (2007).
320 39. Peltier, W. R. & Vettoretti, G. Dansgaard-Oeschger oscillations predicted in a
321 comprehensive model of glacial climate: A 'kicked' salt oscillator in the Atlantic.
322 *Geophys. Res. Lett.* **41,** 7306–7313 (2014).
323 40. Schmittner, A. & Galbraith, E. D. Glacial greenhouse-gas fluctuations controlled by
324 ocean circulation changes. *Nature* **456,** 373–376 (2008).

325 **Acknowledgements:** X.Z. thanks G. Leduc for helpful discussion about marine sediment core
326 MD02-2529. We thank colleagues in Paleoclimate Dynamics group at the Alfred Wegener
327 Institute Helmholtz Center for Polar and Marine Research (AWI) in Bremerhaven for general
328 support and the AWI computer center to keep the supercomputer running. This study is
329 supported by Helmholtz Postdoc Program (PD-301), as well as the PACES program of the AWI
330 and the BMBF funded project PalMod. The opening foundations of the Key Laboratory of
331 Marine Sedimentology & Environmental Geology, SOA, (grant No. MASEG201701) and State
332 Key Laboratory of Marine Geology, Tongji University (grant No. MGK1611) as well as the
333 national Natural Science Foundation of China (grant No. 41575067) are grateful acknowledged
334 (X.Z.). Furthermore, G.K. acknowledges funding by 'Helmholtz Climate Initiative REKLIM'
335 (Regional Climate Change), a joint research project of the Helmholtz Association of German

research centres (HGF). We also acknowledge financial support from the UK NERC (grants NE/J008133/1 and NE/L006405/1) to SB.

Author contributions: All authors conceived the study. X.Z. designed and performed the model simulations, analysed the results, and led the write up of the manuscript with G.K. All authors interpreted the results and contributed to the final version of the manuscript.

Competing financial interests: The authors declare no competing financial interests.

Figure captions:

Figure 1. Transient simulations of the experiment CO2_Hys (left) and LGM_0.15_CO2 (right). (a, h) The CO_2 forcing (ppm); **(b, i)** AMOC index (Sv); **(c, j)** Greenland SAT (°C); **(d, k)** Antarctic (70-80°S zonal mean) SAT index (°C) ; **(e, l)** NENA SIC index (%); **(f, m)** surface salinity anomaly (psu) between the WSNA and EEP; **(g, n)** AMOC-associated MFT[31] (Sv) across 43°N in the North Atlantic. Thin black lines represent the original modeled outputs, and thick red lines in b)-g) and i)-n) are the 100-year and 60-year running means, respectively. Negative model years indicate the control simulations.

Figure 2. AMOC hysteresis and trend analysis in the increasing CO_2 scenario of the experiment CO2_Hys. (a) AMOC hysteresis associated with CO_2 changes. Time points defined in Fig. 1a is shown by letters within which point A and E are indicated by red and blue circles, respectively. **(b-e)** Trend in the CO_2 increasing scenario (interval A-B in a). (b-d) are for sea surface salinity (psu/ka), temperature (℃/ka) and density (kg/m^3/ka), and their vertical profiles over the NENA (as shown by green rectangle in b) are plotted in the upper right corner. **(e)** shows net precipitation (mm/day /ka, shaded), 850hPa wind (m/s /ka, vector), and sea level pressure trend (Pa /ka, contour).

Figure 3. Summary cartoon of the proposed mechanism in this study. (a) Stadial conditions with a relatively low atmospheric CO_2 level, **(b)** stadial conditions with rising CO_2, and **(c)** interstadial conditions with a high CO_2 level. Location of the paleo-salinity record[38] is highlighted by red star in a). Dark dashed lines represent the ITCZ. Interoceanic moisture transport is represented by green arrows, of which thickness schematically indicate the strength of the moisture transport. Red and blue belts/arrows indicate upper northward and deeper southward AMOC branch, respectively. The brown shading represents net evaporation region over the western subtropical North Atlantic.

Figure 4 Synthesis of AMOC stability diagrams. a) CO_2 change-induced diagram under different constant global ice volumes. **b)** ice-volume change-induced diagram under different constant CO_2 levels. The color scheme represents scenarios with a) different ice-volume levels expressed as equivalent sea level (e.s.l.) drops and b) CO_2 levels. Light green curve in (a) represents experiment CO2_Hys, identical to Fig. 2a. Stars are indicative of equilibrium simulations (Table S1) and solid lines represent hysteresis behavior in response to gradual changes in a) atmospheric CO_2 and b) ice volume. Dashed lines in a) and b) represent inferred changes in AMOC strength based on equilibrium simulations performed in this study and 8,9.

Methods:

We use a comprehensive fully coupled atmosphere-ocean general circulation model (AOGCM), COSMOS (ECHAM5-JSBACH-MPIOM) for this study. The atmospheric model ECHAM5[41], complemented by a land surface component JSBACH[42], is used at T31 resolution (~3.75°), with 19 vertical layers. The ocean model MPI-OM[43], including sea ice dynamics that is formulated using viscous-plastic rheology[44], has a resolution of GR30 (3°x1.8°) in the horizontal, with 40 uneven vertical layers. The climate model has already been used to simulate the last millennium[45], the Miocene warm climate[46,47], the Pliocene[48], the internal variability of the climate system[49], Holocene variability[50], the Last Glacial Maximum (LGM) climate[9,51] and

glacial millennial-scale variability[8,52,53]. To evaluate the role of atmospheric CO_2 on the AMOC stability, boundary conditions including ice sheet extent, topography over bare land, orbital configuration, land sea mask, bathymetry, CH_4 and N_2O, are fixed to the LGM. Noted that the imposed ice sheet heights in experiment CO2_Hys and LGM_0.15_CO2 are different. In experiment CO2_Hys the ice volume is equivalent to ~40m sea level drop, while it is identical to the LGM in experiment LGM_0.15_CO2. The ocean states under both ice sheet configurations are characterized by only one stable AMOC mode[8], which enable us verify whether changes in atmospheric CO_2 does play a role on AMOC hysteresis.

Data sources: The data used in this paper are available at the following sources.

Bereiter *et al*. (2015), CO_2 data:

http://onlinelibrary.wiley.com/store/10.1002/2014GL061957/asset/supinfo/grl52461-sup-0003-supplementary.xls?v=1&s=e77ad89c3925111330671009ab40eac65e019d01.

Leduc et al (2007), salinity reconstruction in the eastern Equotorial Pacific:

ftp://ftp.ncdc.noaa.gov/pub/data/paleo/contributions_by_author/leduc2007/leduc2007.txt

Data availability: The model data that support the findings of this study are available from the corresponding author upon reasonable request.

Code availability: The standard model code of the 'Community Earth System Models' (COSMOS) version COSMOS-landveg r2413 (2009) is available upon request from the 'Max Planck Institute for Meteorology' in Hamburg (https://www.mpimet.mpg.de).

References in Methods:

41. Roeckner, E. *et al.* Report No . 349 the atmospheric general circulation model ECHAM5 Part 1: Model description. 1–127 (2003).

42. Brovkin, V., Raddatz, T., Reick, C. H., Claussen, M. & Gayler, V. Global biogeophysical

414 interactions between forest and climate. *Geophys. Res. Lett.* **36,** 1–5 (2009).
415 43. Marsland, S. J., Haak, H., Jungclaus, J. H., Latif, M. & Röske, F. The Max-Planck-
416 Institute global ocean/sea ice model with orthogonal curvilinear coordinates. *Ocean*
417 *Model.* **5,** 91–127 (2003).
418 44. Hibler III, W. A dynamic thermodynamic sea ice model. *J. Phys. Oceanogr.* **9,** 815–846
419 (1979).
420 45. Jungclaus, J. H. *et al.* Climate and carbon-cycle variability over the last millennium.
421 *Clim. Past* **6,** 723–737 (2010).
422 46. Knorr, G., Butzin, M., Micheels, A. & Lohmann, G. A warm Miocene climate at low
423 atmospheric CO 2 levels. *Geophys. Res. Lett.* **38,** 1–5 (2011).
424 47. Knorr, G. & Lohmann, G. Climate warming during Antarctic ice sheet expansion at the
425 Middle Miocene transition. *Nat. Geosci.* **7,** 2–7 (2014).
426 48. Stepanek, C. & Lohmann, G. Modelling mid-Pliocene climate with COSMOS. *Geosci.*
427 *Model Dev.* **5,** 1221–1243 (2012).
428 49. Wei, W., Lohmann, G. & Dima, M. Distinct modes of internal variability in the Global
429 Meridional Overturning Circulation associated with the Southern Hemisphere westerly
430 winds. *J. Phys. Oceanogr.* **42,** 785–801 (2012).
431 50. Wei, W. & Lohmann, G. Simulated Atlantic Multidecadal Oscillation during the
432 Holocene. *J. Clim.* **25,** 6989–7022 (2012).
433 51. Abelmann, A. *et al.* The seasonal sea-ice zone in the glacial Southern Ocean as a carbon
434 sink. *Nat. Commun.* **6,** 8136 (2015).
435 52. Gong, X., Knorr, G., Lohmann, G. & Zhang, X. Dependence of abrupt Atlantic
436 meridional ocean circulation changes on climate background states. *Geophys. Res. Lett.*
437 **40,** 3698–3704 (2013).
438 53. Köhler, P., Knorr, G. & Bard, E. Permafrost thawing as a possible source of abrupt
439 carbon release at the onset of the Bølling/Allerød. *Nat. Commun.* **5,** 5520 (2014).

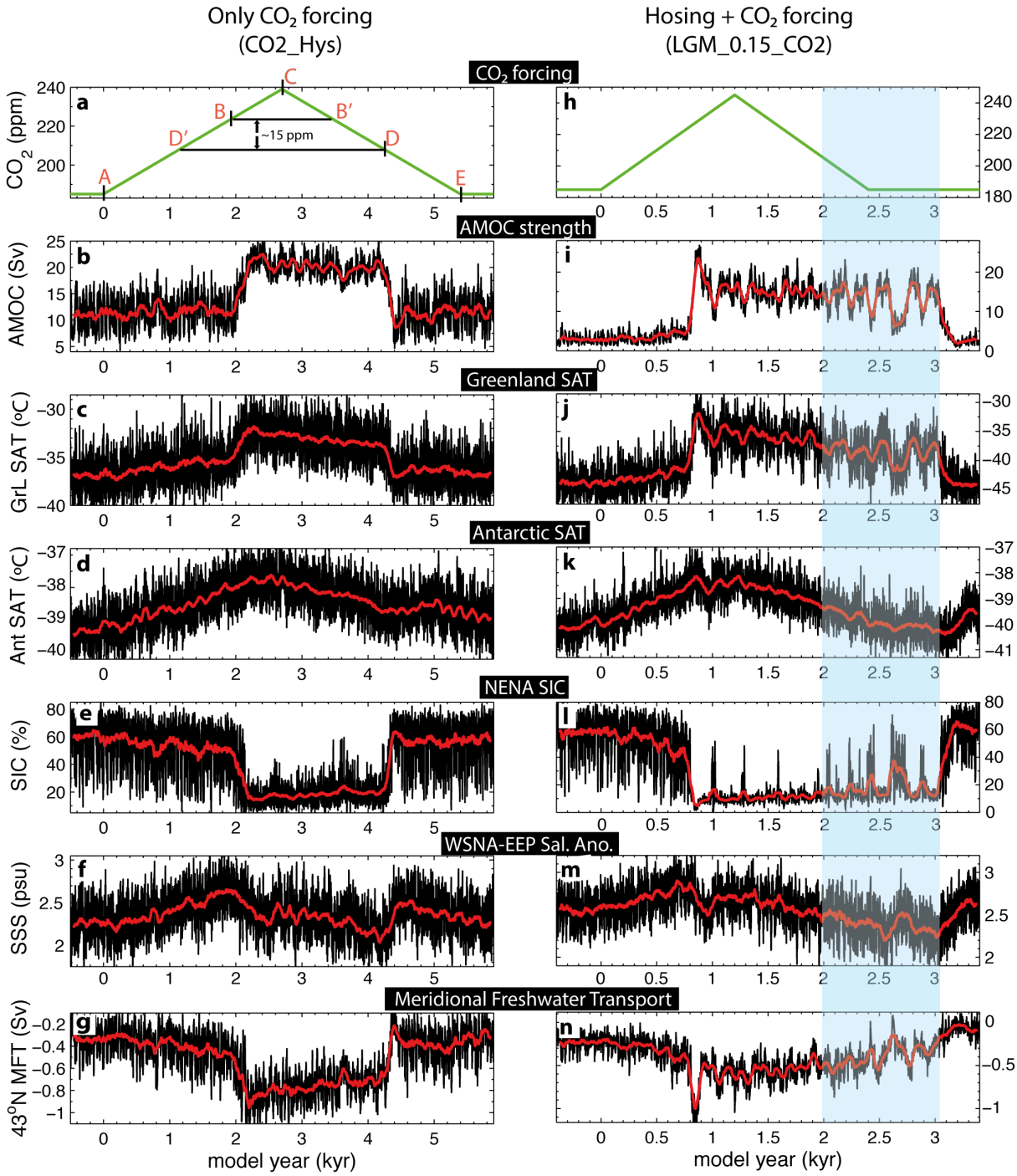

Figure 1. Transient simulations of the experiment CO2_Hys (left) and LGM_0.15_CO2 (right). (a, h)

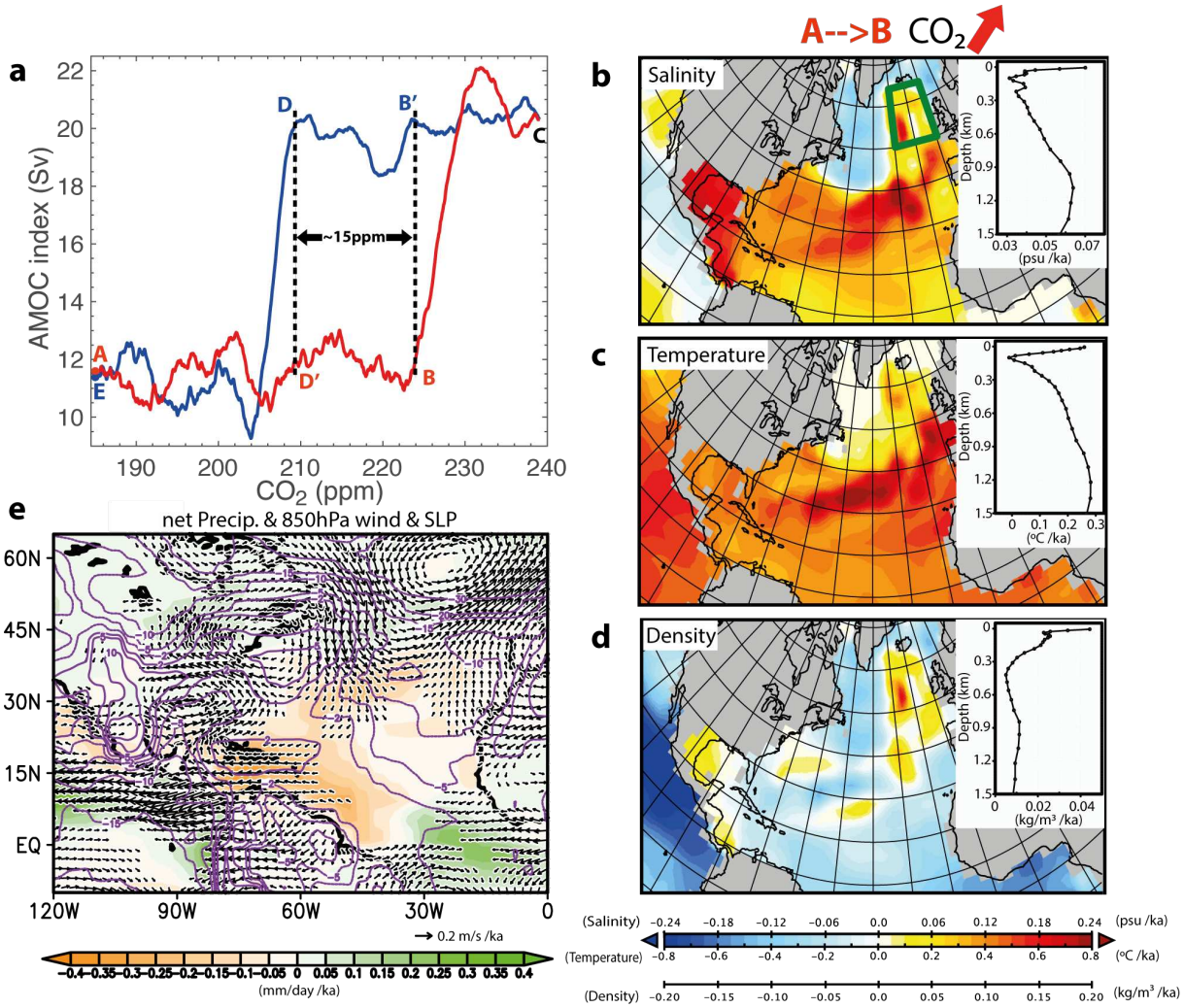

Figure 2. AMOC hysteresis and trend analysis in the increasing CO_2 scenario of the experiment CO2_Hys.

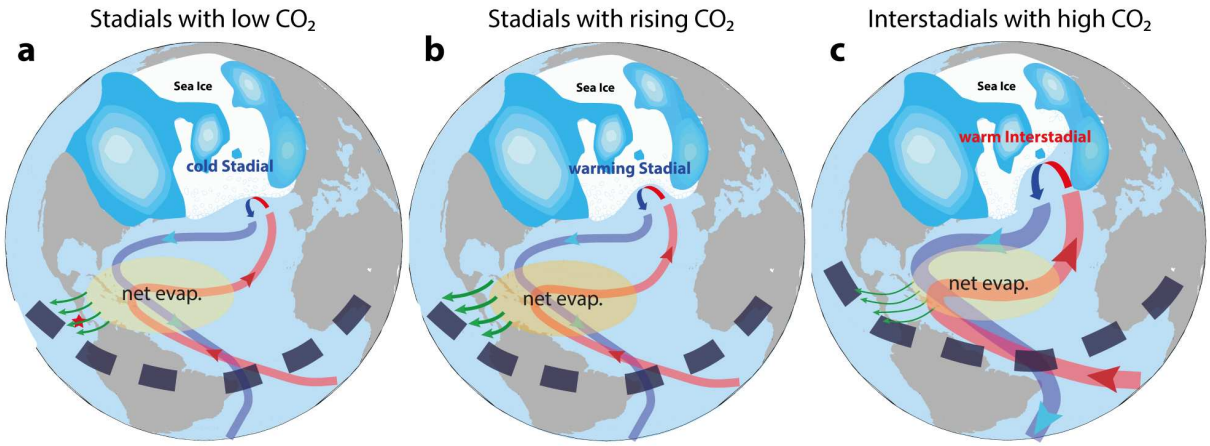

14

15 **Figure 3. Summary cartoon of the proposed mechanism in this study.**

16

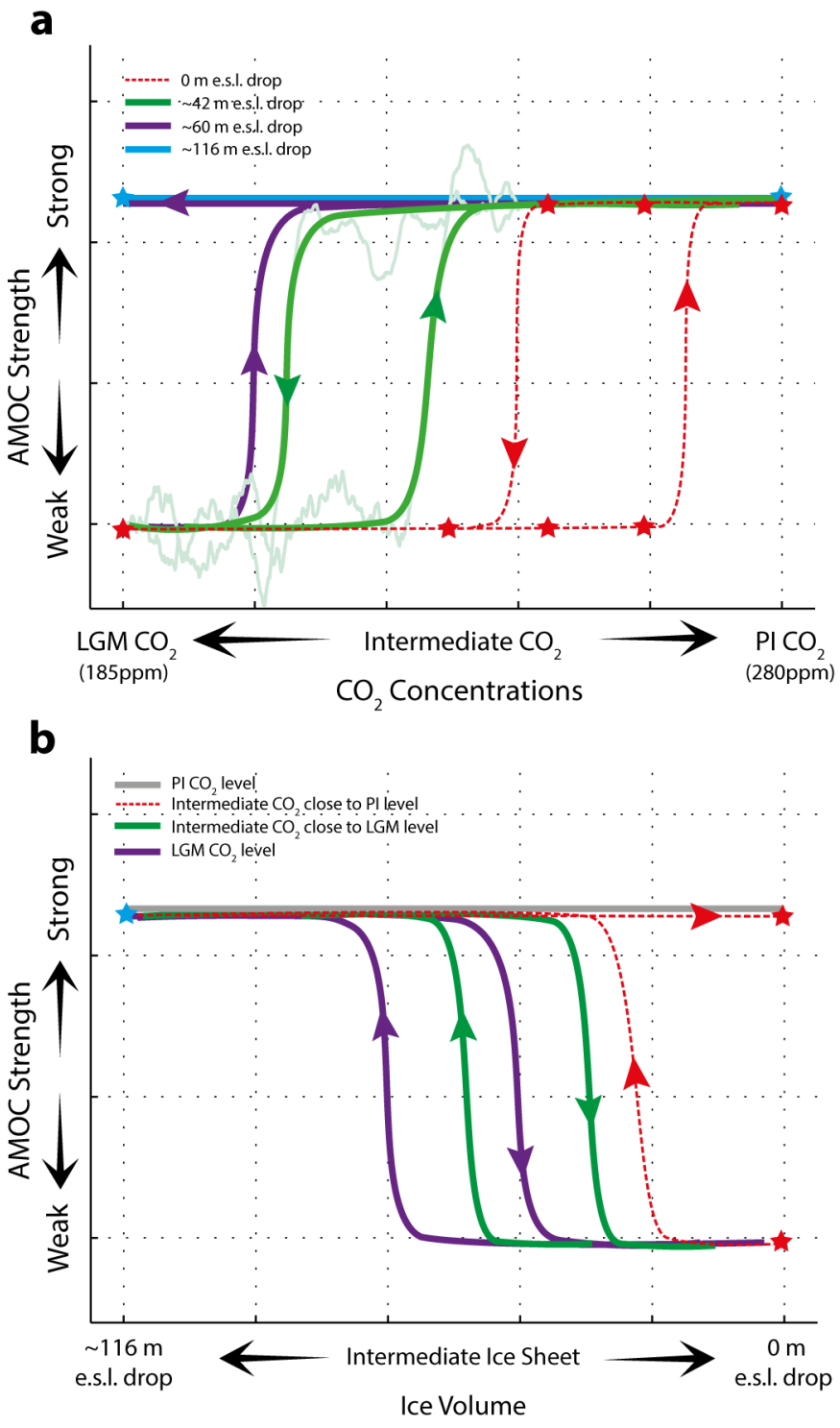

17

18 **Figure 4 Synthesis of AMOC stability diagrams.**